Chemistry—Methods

Research Article
doi.org/10.1002/cmtd.202300044

Chemistry
Europe
European Chemical
Societies Publishing

www.chemistrymethods.org

Versatile spectroscopic cell for *operando* studies in heterogeneous catalysis using tender X-ray spectroscopy in fluorescence mode

H. A. Suarez Orduz,[a, b] S.-L. Heck,[b] P. Dolcet,[b] Y. Watier,[a] M. Casapu,[b] J.-D. Grunwaldt,*[b, c] and P. Glatzel*[a]

The design and commissioning of a cell suitable for *operando* studies using high-energy-resolution fluorescence-detected X-ray absorption near-edge structure (HERFD-XANES) spectroscopy in the tender X-ray regime is reported. The cell is optimized for measurements within the energy range of 1.5 keV to 4.5 keV. It has a plug-flow geometry and can be used for sieved powder samples, analogous to reactors employed for laboratory tests. The functionality of the spectroscopic cell is demonstrated in the area of emission control using CO oxidation as target reaction over 1 wt.% Rh/γ-Al$_2$O$_3$ as catalyst. We show how HERFD-XANES at the Rh L$_3$-edge captures variations in the noble metal structure resulting from the interaction with the support material and reactant molecules. Moreover, distinct structural changes were identified along the catalyst bed as a function of temperature and local gas mixture.

Introduction

Catalysis has been essential for society's development, contributing to the improvement of numerous chemical processes for energy production, pharmaceutical and food industry, or for clean air by lowering harmful emissions.[1] Despite the impressive progress in all these fields, several challenges still need to be faced. The main ones are improved selectivity and higher stability toward catalyst aging or poisoning.[2,3] Herein, tuning and controlling the active site structure is a key,[4,5] especially considering the current difficulties of the catalyst production process: raw materials tend to be less abundant, costly, or difficult to access. These aspects are particularly important for noble metal-based catalysts, which are extensively applied in large-scale applications for air purification including emission control, fine chemistry or fuel cells. Understanding the structure of the active sites and their interaction with the reactant species is crucial for developing catalysts that comply with the current challenges. Considering the dynamic nature of heterogeneous catalysts during variations in gas atmosphere and temperature,[5] their characterization under reaction conditions (*operando*) while monitoring the activity and selectivity is highly important. Additionally, solid structure-activity relationships can be derived for heterogeneous catalysts only under conditions where good contact between the gas flow and catalyst grains is ensured, and bypass of reactants and mass transport limitations are avoided.[6,7]

With respect to the characterization methods, X-ray spectroscopy with synchrotron radiation has proven to be a key technique due to its element selectivity, high penetration depth, and high photon flux that allows the study of the amorphous structure of catalysts under reaction conditions. Such measurements typically provide direct information on the changes in coordination and chemical environment for the atom of interest during variations in the sample environment. The spatial resolution ranging from tens of microns down to 10 nm allows observing the distribution of chemical states of the catalysts during the reaction.[8–13] X-ray spectroscopy has already been widely used to follow catalytic reactions under reaction conditions.[10,14–20] Whereas investigations in the hard X-ray energy range (>4.5 keV) dominate spectroscopic studies, only a few *operando* experiments were conducted in the tender X-ray energy range (1 to 4.5 keV). These lower energies allow to probe L-edges of 4d-transition metals, including the frequently applied noble metals such as Rh and Pd.[21–25] Investigating L-edges instead of K-edges is advantageous because of the smaller lifetime broadening and the fact that the valence orbitals are directly probed via dipole transitions. The smaller line widths make chemical shifts and changes in the white line profile more readily observable. The sharper features also yield

[a] H. A. Suarez Orduz, Dr. Y. Watier, Dr. P. Glatzel
ESRF – The European Synchrotron
71 Avenue des Martyrs, 38000, Grenoble, (France)
E-mail: glatzel@esrf.fr

[b] H. A. Suarez Orduz, S.-L. Heck, Dr. P. Dolcet, Dr. M. Casapu, Prof. Dr. J.-D. Grunwaldt
Institute for Chemical Technology and Polymer Chemistry (ITCP)
Karlsruhe Institute of Technology (KIT)
 Engesserstr. 18/20, 76131, Karlsruhe (Germany)
E-mail: grunwaldt@kit.edu

[c] Prof. Dr. J.-D. Grunwaldt
Institute of Catalysis Research and Technology (IKFT)
Karlsruhe Institute of Technology (KIT)
76344 Eggenstein-Leopoldshafen (Germany)

better sensitivity to mixed species or contaminants, which are generally difficult to detect.[26]

High-energy-resolution fluorescence-detected (HERFD) X-ray absorption near edge structure (XANES) is attracting increasing interest as a tool to follow catalytic processes,[15,27,28] as it increases the spectral resolution and eliminates most background signal.[21,29–32] HERFD-XANES at the L$_3$-edge using the Lα_1 emission lines ($3d_{5/2} \rightarrow 2p_{3/2}$) probes the unoccupied 4d orbitals. The shape of the white line is sensitive to ligand type, bond angles and interatomic distances. Therefore, such studies provide information on the interaction of various ligands with the central atom during reaction.[23–25] The high spectral quality with high spectral resolution and low background is crucial for the identification of complex and possibly small spectral changes. Furthermore, it helps to systematically analyze spectra recorded *operando* that are often a superposition of several species (active site and spectator) with different contributions to the catalytic activity.

The absorption edges and emission lines of 4d transition metals are in the tender X-ray region (1.5 keV–4.5 keV)[33] where the X-ray attenuation is considerably stronger than in the hard X-ray range above 4.5 keV. Alumina as a support material absorbs strongly and emits intense fluorescence lines in the tender X-ray range, while it requires little consideration for measurements at K-edges. An X-ray emission spectrometer installed in a vacuum chamber eliminates any air path and effectively diminishes all unwanted fluorescence lines. The in-vacuum tender X-ray emission spectrometer (TEXS)[33] of beamline ID26 at the ESRF provides the possibility to study the L-edges of 4d transition metals by means of HERFD-XANES. However, for *in situ/operando* studies in the tender X-ray range the design of a suitable cell calls for particular attention. Here we present an *in situ/operando* cell for HERFD-XANES in the tender X-ray range and show the first results obtained for a low loaded Rh/γ-Al$_2$O$_3$ oxidation catalyst for emission control.

Results and Discussion

Description of the spectroscopic in situ/operando cell

Cell requirements

In Table 1 are listed the most crucial aspects for building an *in situ/operando* cell for measurements of heterogeneous catalysts in the tender X-ray energy range. These aspects were selected based on the needs that arise when measurements are conducted in the TEXS of beamline ID26 at the ESRF. It is a compromise between the spectroscopic experiment and the well-known guidelines for catalyst testing.[34]

The *operando* cell is constructed with a plug-flow configuration where the sieved sample is placed between two quartz wool plugs.[35] Plug-flow reactors also promote a fast catalyst response to the change in gas composition because of the small dead volume.[36] Designing a cell with all these characteristics involves important challenges, such as gas tightness, using

Table 1. Key parameters considered for the construction of the *in situ/operando* cell adapted for TEXS at the ESRF beamline ID26.

Aspects	Requirements
Instrumental aspects	1. The aperture angle of the outgoing X-rays should be as large as possible in order to allow the detection of the fluorescence by all TEXS analyzer crystals. 2. The cell must allow measurements across the surface of the catalytic bed: vertically by at least ±0.75 mm and horizontally by at least ±6 mm along the direction of the gas flow through the catalyst bed. 3. An efficient cooling system for the cell with good thermal isolation and shielding is important because high temperatures can damage mechanical components around the furnace and induce high noise in X-ray detectors. With the low pressure inside the chamber, convection is ineffective and heat dissipation occurs only via conduction and radiation.
Window Characteristics	1. The window must exhibit minimal X-ray attenuation of the sample signal. High attenuation would limit the measurement of diluted samples. 2. The window must resist the pressure difference between the catalytic bed (approx. 1 bar) and the pressure inside the TEXS chamber (approx. 1.5×10^{-2} mbar). Furthermore, because of the pressure difference, the window's effective sealing of the catalytic bed is crucial. Consequently, gaskets are necessary to prevent potential leaks of reaction gas into the TEXS chamber. 3. The window must be inert and resistant over a reasonably broad temperature range.
Catalysis requirements	1. Gas flow through the sample and mass transport must be optimized to ensure reaction and flow conditions for the X-ray probed sample volume.[7] 2. Bypass of reactants must be avoided. 3. Cell heating must be spatially uniform and accurate (±1°C) without overshooting. 4. The heat capacity of the cell should be small to allow fast temperature changes. 5. Metals that are studied in the catalyst should not be present in the cell in the vicinity of the sample. 6. Dead volume in the front and after the catalyst bed, as well as before the gas analytics, must be minimal.

materials with low X-ray attenuation, high resistance to large pressure differences, and temperature variations.

The cell design

The *in situ/operando* cell (Figure 1) was developed with the aim to handle a small, lightweight device that can be used in fluorescence mode and ensure proper diffusion of gases through the sample during a catalytic reaction. It is essential to mention that a conventional quartz catalytic reactor is not suitable for the tender x-ray region since quartz is a strongly absorbing material at these energies. The cell body was manufactured through 3D printing via direct metal laser sintering (DMLS) of stainless steel by Protolabs (France). Stainless steel was chosen due to its excellent chemical stability under various reaction conditions. It has a sample channel of 1.5 mm × 1.5 mm × 12 mm dimensions, which is based on the smallest volume that *Hannemann et al.*[37] used for an analogous hard X-ray *operando* cell. In a more advanced version of the cell,
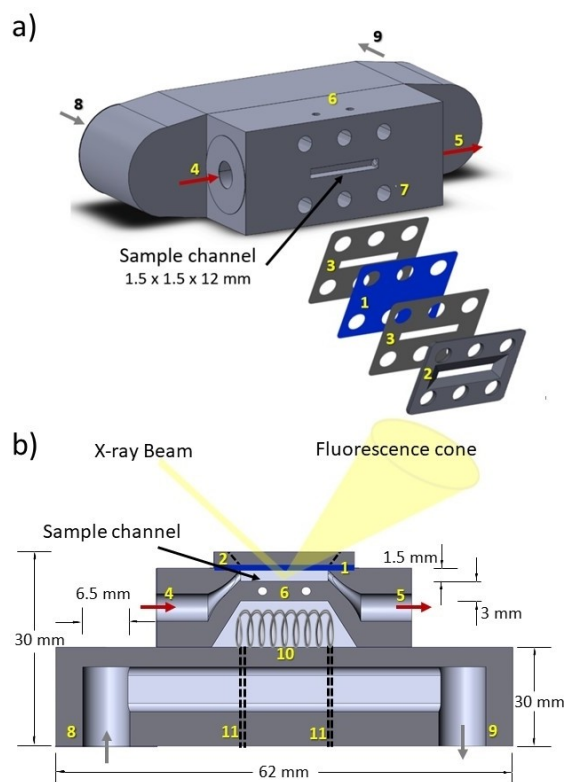
Figure 1. Spectroscopic *in situ/operando* cell for tender X-ray investigations: a) 3D catalytic reactor design with its main parts. b) Longitudinal section of the reactor. 1 – window, 2 – metallic sample cover, 3 – graphite gasket, 4 – gas inlet, 5 – gas outlet, 6 – thermocouples, 7 – screw holes (6 units), 8 – air cooling inlet, 9 – air cooling outlet, 10 – resistor, 11 – electric connections.

the sample channel could have a gold coating or a detachable sample holder made of a different material than stainless steel. This will minimize the signal from elements in stainless steel, such as Fe, Cr, Ni, and Mn.

The cell (Figure 1) has a metallic sample cover attached with six screws on top of the sample. With the help of two 200 μm thick graphite gaskets (manufactured by HPMS graphite), the cover holds the X-ray window. The sieved catalyst powder is positioned in the sample channel between two quartz wool plugs, to prevent catalyst loss or moving of the catalyst bed during experiments. After filling the catalyst grains in the compartment, several graphite pieces as gaskets and the cell window are used to seal the *in situ/operando* cell. The gas dosing system is connected to the cell's inlet and outlet by using Swagelok® fittings. A Kanthal® APM (Advanced Powder Metallurgical) wire resistor provides heating over the whole length of the sample channel. The distance separating the sample from the resistor is 3 mm (Figure 1b), but the heat transfer is efficient due to the high thermal conductivity of stainless steel. Temperature control is performed by two thermocouples located at 1.5 mm from the sample channel. The thermocouple location allows precise reactor temperature control through a Eurotherm nanodac™ recorder/controller. The cell can be heated or cooled at varying ramp rates between 0.5 to 50 °C/min up to 800 °C. However, the temperature range needs to be adjusted in accordance to the material limitations

of the applied cell window and gas atmosphere. The cell is permanently connected to a cooling system (air or water). Additionally, the cell body is on a holder with water cooling via circulation to protect the surrounding components from high temperatures. The holder is attached to a metal stage that can be mounted on the translation stages of the beamline.

For selecting the window material, several criteria were considered. The window material has to be low X-ray absorbing but sufficiently resistant during installation and under reaction conditions. Different graphite foil thicknesses (17, 25, and 40 μm) were tested. We chose a thickness of 25 μm for the *in situ/operando* cell due to its ability to withstand reaction conditions and its moderate attenuation of the sample signal (see Electronic Supplementary Information). The *in situ/operando* cell was installed into the vacuum chamber by using flexible KF25 stainless steel vacuum couplings and DN40CF-DN25KF flange adapters for gas and electrical connections. Figure 2 illustrates the position of the cell inside the TEXS spectrophotometer. The cell is mounted on positioning stages that allow for alignment into the source point of the X-ray emission spectrometer and is rotated at 45 degrees with respect to the incoming beam.

High-resolution infrared thermography was used to assess heating homogeneity in the catalytic channel using a Vario-CAM®hr head camera. Figure 3 shows the uniform heating of the cell, which prevents the formation of hot spots that could affect the chemical reaction. Temperature calibration was achieved by using the two thermocouples installed in the cell and directly measuring the temperature in the sample. To this end, a thermocouple was introduced through the tubing and kept in contact with the sample while a constant flow of 50 mL/min of helium was dosed. The results confirm the thermal reliability and accuracy of the cell over the studied temperature range (see Electronic Supplementary Information).

The *in situ/operando* cell designed showcases several advantages such as optimal gas diffusion that is crucial for operando studies, chemical stability provided by stainless steel construction, and precise temperature control through the use of a Kanthal® APM resistor and thermocouples. Moreover, it ensures heating uniformity, avoiding hot spots, and displays versatility in design, allowing the adaptation of coatings or sample supports in advanced versions.

Application: HERFD-XANES investigations

The suitability of the cell for catalytic *in situ/operando* measurements was tested for a 1 wt. % Rh/γ-Al$_2$O$_3$ catalyst during CO oxidation between 25–350 °C. We collected HERFD-XANES spectra at the Rh L$_3$-edge, which showed clear and distinct spectral features that helped derive structure-activity correlations. However, similarly to most XAS measurements in fluorescence mode, the obtained data suffer from spectral distortions due to over- or self-absorption effects.[38,39] Nonetheless, the influence is negligible for the catalyst studied here because of the low Rh concentration and strongly absorbing Al$_2$O$_3$ in this energy range. The validity of the results obtained

Chemistry—Methods

Research Article
doi.org/10.1002/cmtd.202300044

Chemistry Europe
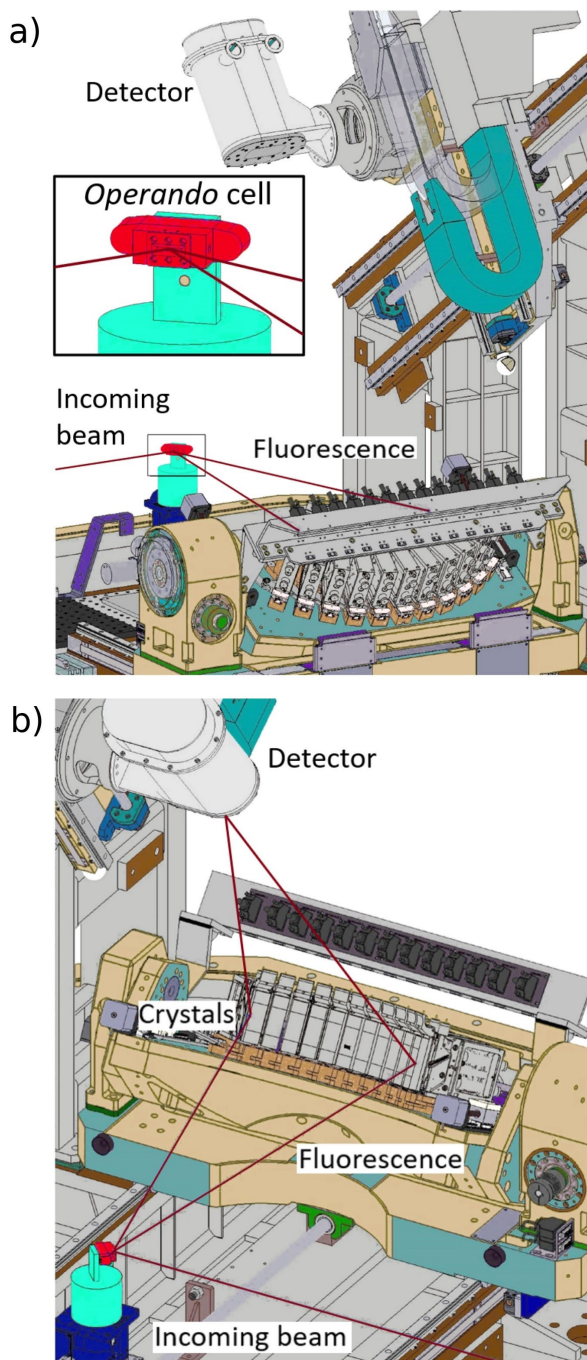European Chemical
Societies Publishing

Figure 2. Positioning of the *in situ/operando* cell inside the TEXS chamber: a) Front view, showing the geometry of the incoming beam in relation to the catalytic channel. b) Posterior lateral view, showing how the crystals focus the fluorescence towards the detector.

with the *in situ/operando* cell was confirmed by comparing the catalytic conversion measured during the HERFD-XANES measurements with the one obtained in a fixed-bed tubular flow reactor, under the same reaction conditions. The consistency in the results highlights the coherence in the dynamics of the reaction investigated, thereby validating the measurements made by HERFD-XANES.
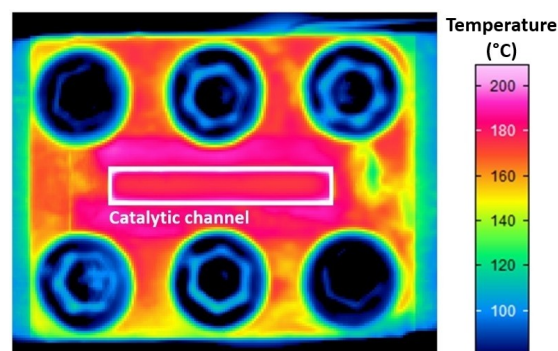

Figure 3. Thermal photograph of the *in situ/operando* cell (front view). The white box underlines the location of the catalyst in the cell channel.

Operando HERFD-XANES measurements during CO oxidation over a 1 wt.% Rh/γ-Al$_2$O$_3$ catalyst

We collected the HERFD-XANES spectra during the following steps: (i) the catalyst in static air at 25 °C; (ii) pre-treatment in 5% O$_2$/He up to 350 °C to remove physiosorbed species and other traces on catalyst surface; (iii) under CO oxidation conditions of 3000 ppm CO, 1.5% O$_2$/He, while heating the catalyst bed by 5 °C/min to 350 °C. The obtained spectra were normalized to the spectral area in the range 3000.00 eV to 3014.00 eV. The area normalization follows the previously reported f-sum rule[40] (more details in Electronic Supplementary Information), ensuring that the system's fundamental properties are reflected, which enables the identification of genuine differences in sample structure while sidelining artefact effects as much as possible. Additionally, we measured a Rh foil to correct the Bragg angle expected for the edge energy of Rh L$_3$-edge (3004 eV).[41]

Figure 4 shows the Rh L$_3$-edge HERFD-XANES spectra measured for the 1 wt.% Rh/γ-Al$_2$O$_3$ catalyst at room temperature after pre-treatment in an oxidative atmosphere and after exposure to the CO containing gas stream inside of the *in situ/operando* cell. Additionally, the spectra collected for Rh foil and pellets of Rh$_2$O$_3$, and RhO$_2$ are shown. To ensure a comparable Rh concentration as in the catalyst and minimize the self-absorption effect in the spectra of Rh$_2$O$_3$ and RhO$_2$, a 1:99 wt.% ratio of cellulose was used as a diluting agent during the measurements for the reference samples. However, some self-absorption for Rh foil measurements has to be considered. One observes strong variations between the white line profiles of the differently treated catalysts, which result from the interaction with the specific gas molecules. Comparison of the HERFD-XANES spectra measured for the Rh/γ-Al$_2$O$_3$ catalyst inside of the *in situ/operando* cell indicates a similar data quality as that obtained for the pellets of Rh reference compounds measured without the cell. With respect to the local structure, a shift of the white line towards higher energy is observed for the alumina supported catalyst in comparison to the RhO$_2$ and Rh$_2$O$_3$ references. Previous investigations have shown that the exposure of Rh/γ-Al$_2$O$_3$ to high temperatures under oxidizing atmosphere leads to highly dispersed noble metal species.
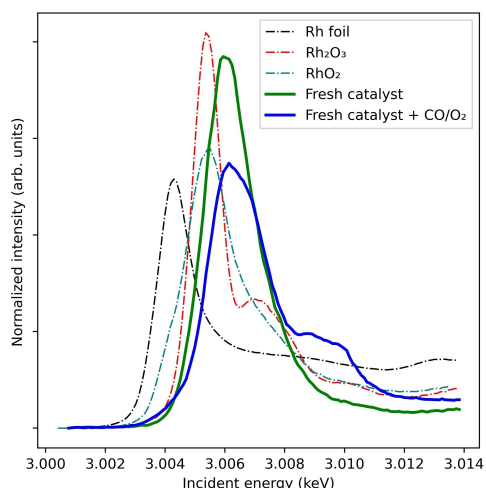
Figure 4. Rh L_3-edge HERFD-XANES spectra for 1 wt.% Rh/γ-Al$_2$O$_3$ fresh catalyst at room temperature after pre-treatment in oxidative atmosphere (green line) and exposure to 3000 ppm CO, 1.5% O$_2$/He at room temperature (blue line). The spectra of Rh$_2$O$_3$, RhO$_2$, and Rh foil references are additionally shown in dot-dashed lines.

Above 600 °C the diffusion of Rh into the subsurface or bulk alumina lattice with the formation of RhAlO$_x$ was reported.[42,43] In highly dispersed state or for low-loaded samples, Rh is located at sublattice octahedral sites of the cubic spinel γ-Al$_2$O$_3$, most probably as Rh^{3+} species. According to our results, this strong interaction with the support affects the electronic configuration of Rh species already for lower catalyst calcination temperatures, i.e. at 500 °C. However, the diffusion of Rh into the alumina lattice is not expected at these temperatures. Despite being present in an oxidized state, the entire Rh L_3 edge profile of the fresh catalyst does not resemble those of Rh$_2$O$_3$ and RhO$_2$ references. Most of the Rh species seem to be accessible on the alumina surface, as they are able to interact with the CO and O$_2$ molecules. This is indicated by the pronounced changes occurring in the HERFD-XANES profile already at room temperature during exposure of the catalyst to

the gas mixture, which is in line with previous infrared spectroscopy studies conducted on similar samples.[44] Depending on the noble metal state and reaction conditions, highly dispersed Rh species (single atoms, clusters or particles) are known to adsorb none, one or two CO molecules.[44–46] CO adsorption on Rh metallic surface involves electron donation from the 5σ-CO molecular orbital to the metal but also back-donation of p and d electrons from Rh to the antibonding 2π* molecular orbital of CO, which weakens the C—O bond. As shown by Schwegmann et al.,[47] the back-donation is diminished if oxygen is co-adsorbed due to its competing effect, leading to a more facile desorption of CO. In our experiment, the noble metal is initially in an oxidized state, and oxygen concentration is in excess relative to CO concentration. For this state, the predominant formation of *gem*-dicarbonyls Rh$^{\delta+}$(CO)$_2$ or linearly bound CO species is expected at room temperature.[48–50] The decrease of the white line intensity indicates a partial reduction from Rh^{3+} to Rh$^+$ that occurs already at this low temperature, whereas the new feature appearing at 3009.5 eV is assigned to rhodium carbonyl formation. This slight pre-reduction of highly oxidized Rh species with a change in coordination seems to be mandatory for CO adsorption.[51] Previous diffuse reflectance infrared Fourier transform spectroscopy (DRIFTS) investigations of the surface species formed during CO oxidation over Rh/γ-Al$_2$O$_3$ suggested that CO adsorbed on Rh sites in a higher oxidation state as *gem*-dicarbonyl species are not active for CO oxidation[50,52] In contrast, linear CO adsorbed species formed on Rh clusters and particles show a higher reactivity.[49]

These assignments are in line with the changes observed in the HERFD-XANES spectra collected at the inlet, middle, and outlet positions of the catalyst bed during heating from 100 °C to 350 °C (Figure 5). In comparison to the spectra measured at room temperature for the catalyst in fresh state and after exposure to CO, the white line intensity recovered to some extent after heating in the reaction mixture to 100 °C whereas the shoulder at 3009.5 eV diminished, which is most probably due to partial CO desorption. Nonetheless, the reaction is still
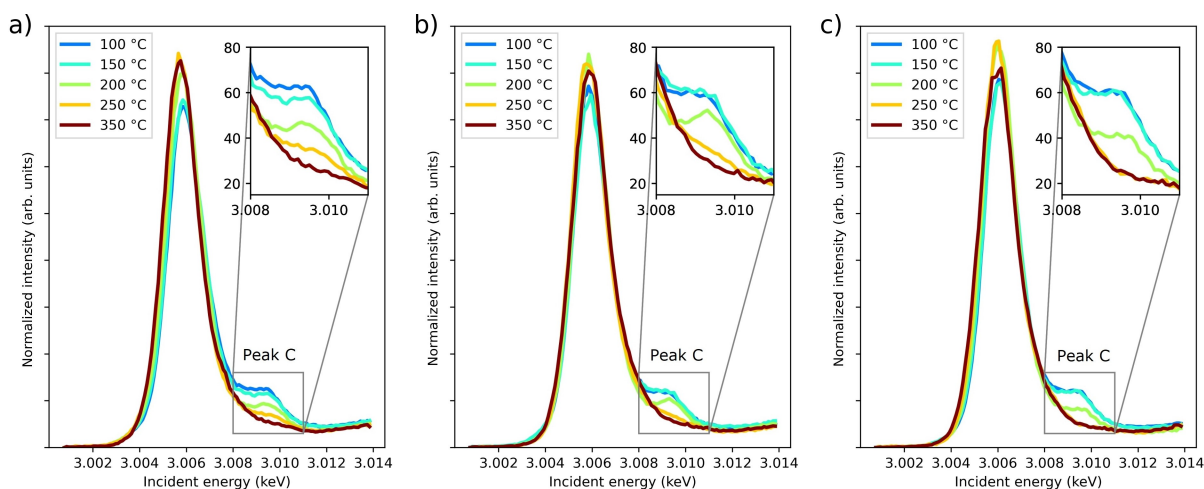

Figure 5. Rh L_3-edge HERFD-XANES spectra collected during the CO oxidation catalytic light-off cycle between 100 °C and 350 °C for 1wt. % Rh/γ-Al$_2$O$_3$. **a)** inlet position, **b)** middle position, **c)** outlet position of the catalyst bed. The inset shows peak C.

Chemistry—Methods

Research Article
doi.org/10.1002/cmtd.202300044

Chemistry Europe
European Chemical
Societies Publishing

inhibited by the remaining rhodium carbonyl species as the CO oxidation onset occurs only above 170 °C (Figure 6). In line with a Langmuir–Hinshelwood reaction mechanism, partial CO desorption is required to allow adsorption and activation of O_2.[48,53] At 250 °C, corresponding to 100 % CO conversion, the fingerprint of rhodium carbonyls is observed only for the inlet and mid position of the catalyst bed. For even higher temperatures, the increase of the reaction rate further shrinks the CO conversion zone towards inlet positions in the catalyst bed,[54,55] as indicated by the remaining small shoulder at 3009.50 eV in the HERFD-XANES spectra measured at the inlet position.

Each HERFD-XANES spectrum in Figure 5 was fitted with three Voigt functions and an arctangent curve to model the absorption edge step within the 3000.00 eV to 3014.00 eV range. This approach was chosen due to the complexity of the spectra at the Rh L_3 edge, which arises from multiple coordination environments, variations in electronic states, and subtle electronic structure details, making Voigt functions crucial for capturing these intricacies (see Electronic Supplementary Information). In Figure 6, the ratio of the area under peak C at different temperatures to the respective area of the fresh catalyst for the inlet, middle, and outlet positions is shown on the primary y-axis. This ratio is used to reduce any distortions in the spectra that may be caused by various factors such as the sample filling of the *in situ/operando* cell channel. The fingerprint of rhodium carbonyl presence ($Rh^{\delta+}$ in Figure 6) is identified at the outlet and mid positions especially at temperatures below the reaction onset (< 200 °C) whereas the formation of these species is found at the beginning of the catalyst bed even for complete CO conversion. Hence, the obtained results allow a direct correlation between the catalyst structure along the catalyst bed and the measured CO oxidation activity at various temperatures, demonstrating the suitability of the *operando* cell for such studies.
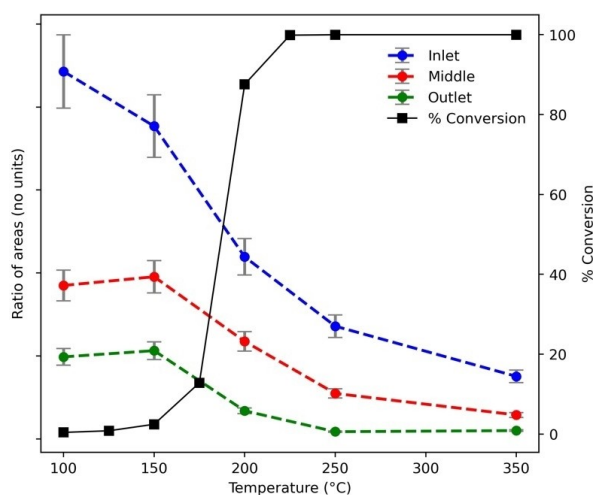

Figure 6. Catalytic activity evaluation through Rh L_3 HERFD-XANES: Spectral area for peak C, normalized to the area of the fresh catalyst at the inlet, middle, and outlet positions of the catalyst bed, is plotted on the primary y-axis. Simultaneously, CO oxidation activity between 100 °C and 350 °C for 1 wt.% Rh/γ-Al_2O_3 is illustrated on the secondary y-axis.

Conclusions

An *in situ/operando* cell was developed for tender X-ray emission measurements and commissioned at the insertion device beamline ID26 (ESRF). The system allows the dosage of different gas mixtures. Simultaneously, the catalyst bed can be heated or cooled in a temperature range of 25–800 °C. The plug-flow geometry of the cell with a catalyst bed containing a sieved powder fraction is analogous to typical laboratory reactors for catalyst tests. The low limit of the energy range used for investigations is given by the X-ray spectrometer, which starts with Al Kα and covers Si, P, S, and Cl as well as the L edges of 4d transition metals.

Variations in the Rh L_3 HERFD-XANES spectral features can be clearly identified during CO oxidation despite the low noble metal loading of 1 wt.%, as illustrated for a Rh/γ-Al_2O_3 catalyst. Furthermore, HERFD-XANES spectra can be collected in a spatially resolved manner along the catalyst bed, allowing to derive accurate structure-activity correlations.

Without further modifications, the *in situ/operando* cell can be used for similar studies on heterogeneous catalysts under transient or steady-state reaction conditions. This opens the way for a large number of experiments in the tender X-ray range for the study 4d transition metals but also phosphorus, sulphur and chlorine. In order to minimize down-time when changing the catalyst, we are currently working on the design of a new cell with three reactors. Additionally, we aim to expand the capabilities of our *in situ/operando* cell to encompass higher temperatures and optimize thermal modulation. With the incorporation of gold coatings, we seek to facilitate the study of iron-based catalysts. Moreover, we are considering adaptations for operations under high pressures and the possible integration with techniques such as extended X-ray absorption fine structure (EXAFS). These advancements will guide us towards a deeper understanding of high-temperature reactions and catalyst deactivation using the advantageous L_3-edge spectroscopy of 4d-transition metals. Finally, the experience gained in the present work will help in the construction of cells for other types of *in situ* studies, for example, in electrocatalysis.

Experimental

HERFD-XANES measurements were carried out using the TEXS installed at beamline ID26 of the ESRF. The incident energy was selected by means of the Si(111) reflection of a double crystal monochromator. The total flux was approximately 10^{13} photons/second using the fundamental harmonic. The size of the beam (Full Width at Half Maximum, horizontal × vertical) was 247 μm × 38 μm. The incoming monochromatic X-ray flux was recorded by detecting the X-ray scattering from a Kapton foil on a photodiode. A metallic foil of Rh was used for incident beam energy calibration. Five Si(111) Johansson crystals analyzers were used in the TEXS chamber. The fluorescence intensity was recorded using a gas proportional counter. HERFD-XANES spectra were recorded by monitoring the fluorescence intensity at the maximum of the Rh $L\alpha_1$ emission line (2696.80 eV) corresponding to a Bragg angle of 47.15 degrees. The samples were checked for radiation damage by

Chemistry—Methods

Research Article
doi.org/10.1002/cmtd.202300044

Chemistry Europe
European Chemical
Societies Publishing

recording 10 consecutive XAS scans (on-the-fly data acquisition) of 30 seconds each. None of the compounds were found to be radiation sensitive.

The 1 wt.% Rh/γ-Al$_2$O$_3$ catalyst was prepared by the incipient wetness impregnation (IWI) method using a 10% rhodium (III) nitrate aqueous solution (Acros Organics) as Rh precursor and commercial γ-Al$_2$O$_3$ (SASOL Germany GmbH) as support. After impregnation, the sample was calcined at 500°C for 5 hours in static air. This resulted in the formation of highly dispersed rhodium nanoparticles with sizes around 1–2 nm. The 1 wt.% Rh/γ-Al$_2$O$_3$ catalyst was sieved to obtain a grain size between 125 μm to 250 μm, which was placed between two quartz wool plugs inside of the *in situ/operando* cell channel. The catalyst bed length was about 6 mm, and 8 mg of catalyst was used. Once the sample was located, the reactor was sealed by positioning the 25 μm graphite window, graphite gaskets and metallic sample cover. The reaction was followed between 25°C to 350°C using the T/C$_1$ and T/C$_2$ thermocouples (at atmospheric pressure, the working temperature range can be extended to 25–800°C). The heating temperature ramp was 5°C/min. Catalytic activity was evaluated by feeding a gas mixture of 3000 ppm CO, and 1.5% O$_2$ in He as balance at a total gas flow rate of 50 mL/min. All gases were dosed through mass flow controllers (Bronkhorst). The resulting reaction products were analyzed with a mass spectrometer (MS, Pfeiffer Vacuum, OmniStar GSD 320 O) and a Fourier transform infrared spectrometer (FTIR, MKS, Multigas MG2030). The MS and FTIR were placed as close as possible to the *in situ/operando* cell to minimize dead volume effects.

Conflict of Interests

The authors declare no conflict of interest.

Data Availability Statement

Research data are not shared.

[1] S. Wacławek, V. V. T. Padil, M. Černík, *Ecol. Chem. Eng. S.* **2018**, *25*, 9–34.
[2] T. J. Schwartz, B. J. O'neill, B. H. Shanks, J. A. Dumesic, *ACS Catal.* **2014**, *4*, 2060–2069.
[3] K. F. Kalz, R. Kraehnert, M. Dvoyashkin, R. Dittmeyer, R. Gläser, U. Krewer, K. Reuter, J.-D. Grunwaldt, *ChemCatChem* **2017**, *9*, 17–29.
[4] J. Bao, G. Yang, Y. Yoneyama, N. Tsubaki, *ACS Catal.* **2019**, *9*, 3026–3053.
[5] A. M. Gänzler, M. Casapu, P. Vernoux, S. Loridant, F. J. Cadete Santos Aires, T. Epicier, B. Betz, R. Hoyer, J.-D. Grunwaldt, *Angew. Chem. Int. Ed.* **2017**, *56*, 13078–13082.
[6] D. E. Doronkin, H. Lichtenberg, J.-D. Grunwaldt, *Cell Designs for In Situ and Operando Studies*, Springer, Cham, **2017**.
[7] J.-D. Grunwaldt, M. Caravati, S. Hannemann, A. Baiker, *Phys. Chem. Chem. Phys.* **2004**, *6*, 3037–3047.
[8] F. Baudelet, R. Belkhou, V. Briois, A. Coati, P. Dumas, V. H. Etgens, A. M. Flank, P. Fontaine, Y. Garreau, O. Lyon, I. Quinkal, F. Rochet, P. Roy, M. Sauvage, F. Sirotti, A. Somogyi, D. Thiaudière, *Oil Gas Sci. Technol.* **2005**, *60*, 849–874.
[9] C. L. Dong, L. Vayssieres, *Chem. Eur. J.* **2018**, *24*, 18356–18373.
[10] J.-D. Grunwaldt, J. B. Wagner, R. E. Dunin-Borkowski, *ChemCatChem* **2013**, *5*, 62–80.
[11] B. B. Sarma, F. Maurer, D. E. Doronkin, J.-D. Grunwaldt, *Chem. Rev.* **2023**, *123*, 379–444.
[12] X. Li, X. Yang, J. Zhang, Y. Huang, B. Liu, *ACS Catal.* **2019**, *9*, 2521–2531.
[13] A. A. Guda, S. A. Guda, K. A. Lomachenko, M. A. Soldatov, I. A. Pankin, A. V. Soldatov, L. Braglia, A. L. Bugaev, A. Martini, M. Signorile, E. Groppo, A. Piovano, E. Borfecchia, C. Lamberti, *Catal. Today* **2019**, *336*, 3–21.
[14] M. A. Newton, *Catalysts* **2017**, *7*, 58.
[15] F. Maurer, J. Jelic, J. Wang, A. Gänzler, P. Dolcet, C. Wöll, Y. Wang, F. Studt, M. Casapu, J.-D. Grunwaldt, *Nat. Catal.* **2020**, *3*, 824–833.
[16] A. Boubnov, H. W. P. Carvalho, D. E. Doronkin, T. Gunter, E. Gallo, A. J. Atkins, C. R. Jacob, J.-D. Grunwaldt, *J. Am. Chem. Soc.* **2014**, *136*, 13006–13015.
[17] S. Yao, K. Mudiyanselage, W. Xu, A. C. Johnston-Peck, J. C. Hanson, T. Wu, D. Stacchiola, J. A. Rodriguez, H. Zhao, K. A. Beyer, K. W. Chapman, P. J. Chupas, A. Martínez-Arias, R. Si, T. B. Bolin, W. Liu, S. D. Senanayake, *ACS Catal.* **2014**, *4*, 1650–1661.
[18] A. Tsoukalou, P. M. Abdala, D. Stoian, X. Huang, M. G. Willinger, A. Fedorov, C. R. Müller, *J. Am. Chem. Soc.* **2019**, *141*, 13497–13505.
[19] K. A. Lomachenko, E. Borfecchia, C. Negri, G. Berlier, C. Lamberti, P. Beato, H. Falsig, S. Bordiga, *J. Am. Chem. Soc.* **2016**, *138*, 12025–12028.
[20] F. Wang, S. He, H. Chen, B. Wang, L. Zheng, M. Wei, D. G. Evans, X. Duan, *J. Am. Chem. Soc.* **2016**, *138*, 6298–6305.
[21] K. I. Shimizu, Y. Kamiya, K. Osaki, H. Yoshida, A. Satsuma, *Catal. Sci. Technol.* **2012**, *2*, 767–772.
[22] K. I. Shimizu, T. Oda, Y. Sakamoto, Y. Kamiya, H. Yoshida, A. Satsuma, *Appl. Catal. B* **2012**, *111–112*, 509–514.
[23] A. Svyazhin, V. Nalbandyan, M. Rovezzi, A. Chumakova, B. Detlefs, A. A. Guda, A. Santambrogio, A. Manceau, P. Glatzel, *Inorg. Chem.* **2022**, *61*, 869–881.
[24] M. W. Tew, J. T. Miller, J. A. Van Bokhoven, *J. Phys. Chem. C* **2009**, *113*, 15140–15147.
[25] M. W. Tew, M. Nachtegaal, M. Janousch, T. Huthwelker, J. A. Van Bokhoven, *Phys. Chem. Chem. Phys.* **2012**, *14*, 5761–5768.
[26] G. N. George, W. E. Cleland, J. H. Enemark, C. A. Kipke, S. A. Roberts, B. E. Smith, S. P. Cramer, *J. Am. Chem. Soc.* **1990**, *112*, 2541–2548.
[27] A. M. Gänzler, M. Casapu, D. E. Doronkin, F. Maurer, P. Lott, P. Glatzel, M. Votsmeier, O. Deutschmann, J.-D. Grunwaldt, *J. Phys. Chem. Lett.* **2019**, *10*, 7698–7705.
[28] D. Friebel, M. W. Louie, M. Bajdich, K. E. Sanwald, Y. Cai, A. M. Wise, M. J. Cheng, D. Sokaras, T. C. Weng, R. Alonso-Mori, R. C. Davis, J. R. Bargar, J. K. Nørskov, A. Nilsson, A. T. Bell, *J. Am. Chem. Soc.* **2015**, *137*, 1305–1313.
[29] P. Glatzel, M. Sikora, G. Smolentsev, M. Fernández-García, *Catal. Today* **2009**, *145*, 294–299.
[30] P. Glatzel, U. Bergmann, *Coord. Chem. Rev.* **2005**, *249*, 65–95.
[31] P. Glatzel, T. C. Weng, K. Kvashnina, J. Swarbrick, M. Sikora, E. Gallo, N. Smolentsev, R. A. Mori, *J. Electron Spectrosc. Relat. Phenom.* **2013**, *188*, 17–25.
[32] S. Lafuerza, M. Retegan, B. Detlefs, R. Chatterjee, V. Yachandra, J. Yano, P. Glatzel, *Nanoscale* **2020**, *12*, 16270–16284.

[33] M. Rovezzi, A. Harris, B. Detlefs, T. Bohdan, A. Svyazhin, A. Santambrogio, D. Degler, R. Baran, B. Reynier, P. N. Crespo, C. Heyman, H. P. Van Der Kleij, P. Van Vaerenbergh, P. Marion, H. Vitoux, C. Lapras, R. Verbeni, M. M. Kocsis, A. Manceau, P. Glatzel, *J. Synchrotron Radiat.* **2020**, *27*, 813–826.

[34] F. M. Dautzenberg, in *ACS Symp. Ser.* (Eds.: S. A. Bradley, M. J. Gattuso, J. Bertolacini), American Chemical Society, Washington DC, **1989**, pp. 99–119.

[35] D. Eggart, A. Zimina, G. Cavusoglu, M. Casapu, D. E. Doronkin, K. A. Lomachenko, J.-D. Grunwaldt, *Rev. Sci. Instrum.* **2021**, *92*, 023106.

[36] G. Agostini, D. Meira, M. Monte, H. Vitoux, A. Iglesias-Juez, M. Fernandez-Garcia, O. Mathon, F. Meunier, G. Berruyer, F. Perrin, S. Pasternak, T. Mairs, S. Pascarelli, B. Gorges, *J. Synchrotron Radiat.* **2018**, *25*, 1745–1752.

[37] S. Hannemann, M. Casapu, J.-D. Grunwaldt, P. Haider, P. Trüssel, A. Baiker, E. Welter, *J. Synchrotron Radiat.* **2007**, *14*, 345–354.

[38] M. Bianchini, P. Glatzel, *J. Synchrotron Radiat.* **2012**, *19*, 911–919.

[39] A. Manceau, M. A. Marcus, N. Tamura, *Rev. Mineral. Geochem.* **2002**, *49*, 341–428.

[40] D. L. Johnson, *Phys. Rev. B* **1974**, *9*, 4475.

[41] A. Thompson, D. Attwood, E. Gullikson, M. Howells, K. Kim, J. Kirz, J. Kortright, I. Lindau, P. Pianetta, A. Robinson, *X-Ray Data Booklet*, Lawrence Berkeley National Laboratory, University Of California Berkeley, CA, Berkeley, **2009**.

[42] C. H. Li, J. Wu, A. B. Getsoian, G. Cavataio, J. R. Jinschek, *Chem. Mater.* **2022**, *34*, 2123–2132.

[43] H. C. Yao, S. Japar, M. Shelef, *J. Catal.* **1977**, *50*, 407–418.

[44] F. C. Meunier, *J. Phys. Chem. C* **2021**, *125*, 21810–21823.

[45] J.-D. Grunwaldt, L. Basini, B. S. Clausen, *J. Catal.* **2001**, *200*, 321–329.

[46] B. B. Sarma, J. Jelic, D. Neukum, D. E. Doronkin, X. Huang, F. Studt, J.-D. Grunwaldt, *J. Phys. Chem. C* **2023**, *127*, 3046.

[47] S. Schwegmann, H. Over, V. De Renzi, G. Ertl, *Surf. Sci.* **1997**, *375*, 91–106.

[48] S. Marino, L. Wei, M. Cortes-Reyes, Y. Cheng, P. Laing, G. Cavataio, C. Paolucci, W. Epling, *JACS Au* **2023**, *3*, 459–467.

[49] D. A. Bulushev, G. F. Froment, *J. Mol. Catal. A* **1999**, *139*, 63–72.

[50] J. A. Andersont, *J. Chem. Soc. Faraday Trans.* **1991**, *87*, 3907–3911.

[51] Y. Tang, C. Asokan, M. Xu, G. W. Graham, X. Pan, P. Christopher, J. Li, P. Sautet, *Nat. Commun.* **2019**, *10*, 1–10.

[52] S. J. A. Figueroa, M. A. Newton, *J. Catal.* **2014**, 69–77.

[53] S. H. Oh, C. C. Eickel, *J. Catal.* **1991**, *128*, 526–536.

[54] S. Hannemann, J.-D. Grunwaldt, N. van Vegten, A. Baiker, P. Boye, C. G. Schroer, *Catal. Today* **2007**, *126*, 54–63.

[55] A. M. Gänzler, M. Casapu, A. Boubnov, O. Müller, S. Conrad, H. Lichtenberg, R. Frahm, J.-D. Grunwaldt, *J. Catal.* **2015**, *328*, 216–224.

RESEARCH ARTICLE

Utilizing a customized *in situ/ operando* cell designed for X-ray spectroscopy in the tender X-ray range, an investigation is reported that unraveled the interactions between the noble metal, support, and reactive molecules throughout the catalytic bed. The *in situ/operando* cell allows the study of dynamic structural changes in heterogeneous catalysts, in this example case in the field of emission control catalysis.
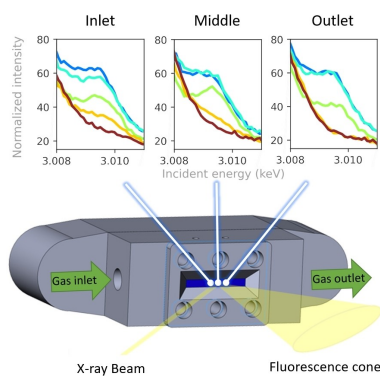
H. A. Suarez Orduz, S.-L. Heck, Dr. P. Dolcet, Dr. Y. Watier, Dr. M. Casapu, Prof. Dr. J.-D. Grunwaldt*, Dr. P. Glatzel*

1 – 9

Versatile spectroscopic cell for *operando* studies in heterogeneous catalysis using tender X-ray spectroscopy in fluorescence mode